INORGANIC CHEMISTRY FRONTIERS

RESEARCH ARTICLE

View Article Online
View Journal | View Issue

Cite this: *Inorg. Chem. Front.*, 2025, **12**, 630

Chemical substitution towards a rare-earth borate ultraviolet NLO crystal exhibiting a strong SHG response†

Xianghao Kong, Jing Chai, Huijian Zhao, Ning Ye, Zhanggui Hu, Yicheng Wu and Conggang Li *

The fabrication of nonlinear optical (NLO) materials that exhibit both a pronounced second harmonic generation (SHG) response and a broad ultraviolet (UV) transmission range remains a big challenge. In this study, we employed a flux method to extract a potential rare-earth borate UV NLO crystal, $K_{7.5}Lu_{2.5}B_{15}O_{30}$, by the chemical cosubstitution strategy. The title compound crystallizes in the trigonal space group *R*32 (no. 155) with a three-dimensional structural framework consisting of $[B_5O_{10}]$ and $[LuO_6]$ groups. Remarkably, $K_{7.5}Lu_{2.5}B_{15}O_{30}$ possesses a notably short cutoff edge of 198 nm and a wide band gap of 6.3 eV. Moreover, it demonstrates a strong phase-matched SHG efficiency of 1.2 × KDP, which represents an optimal balance between a strong NLO effect and a wide UV transmission range. Besides, theoretical calculations and structural analyses unveil that the NLO properties observed in $K_{7.5}Lu_{2.5}B_{15}O_{30}$ are primarily attributable to the synergistic effect of the $[B_5O_{10}]$ groups and $[LuO_6]$ octahedra. These findings indicate that $K_{7.5}Lu_{2.5}B_{15}O_{30}$ has potential applications as beryllium-free UV NLO materials.

Received 30th September 2024,
Accepted 21st November 2024

DOI: 10.1039/d4qi02469a

rsc.li/frontiers-inorganic

Introduction

Ultraviolet (UV) nonlinear optical (NLO) materials, with the ability to generate coherent UV light by laser frequency conversion, are in high demand for versatile advanced applications such as laser photolithography, laser medicine, and semiconductor manufacturing.[1–6] Currently, $KBe_2BO_3F_2$ (KBBF) crystals stand as the only material capable of generating deep-UV laser output through direct frequency doubling. However, the toxicity of beryllium, the raw material used for KBBF, along with the undesirable delamination growth habit, have significantly impeded its extensive utilization.[7–9] Consequently, the pursuit of novel deep-UV and UV NLO crystalline materials represents a formidable challenge. To fabricate short-wave UV NLO crystals, apart from the prerequisite of a non-centrosymmetric (NCS) structure, a wide UV transmission window and a large second-harmonic generation (SHG) response are necessary. Nevertheless, the paradoxical nature of the SHG coefficients and the bandgap correlation function poses a significant challenge in simultaneously achieving strong SHG effects (>1 × KDP) and short UV cutoff edges (<200 nm).[10–12] To address this challenge, effective methods have been employed, such as incorporating NLO-active chromophores as fundamental building blocks (FBBs), including second-order Jahn–Teller (SOJT) effect d^0 transition-metal cations (*e.g.*, Ti^{4+}, Nb^{5+}, *etc.*) with octahedral coordination and post major group metal cations (*e.g.*, Bi^{3+}, Te^{4+}, Sn^{2+}, *etc.*) with stereo-chemically active lone pairs.[13–16] However, the presence of these metal cations always results in unfavorable red shifts at the UV cutoff edge, rendering the materials unsuitable for NLO applications in the UV and deep-UV region.

Borate-based NLO materials have garnered significant interest due to their diverse NCS geometries, obvious NLO responses, excellent thermochemical stability, wide bandgaps, and high transparency, particularly in the UV wavelength range.[17–20] Notably, several borate UV NLO crystals, including LiB_3O_5 (LBO),[21] β-BaB_2O_4 (β-BBO),[22] CsB_3O_5 (CBO),[23] and $CsLiB_6O_{10}$ (CLBO),[24] have been identified as excellent candidates with remarkable overall performance. The overlapping of boron atomic orbitals is well recognized for its ability to generate sp, sp^2, and sp^3 hybrid orbitals, resulting in the formation of three fundamental building blocks (FBBs) in borates: linear $[BO_2]^-$, triangular $[BO_3]^{3-}$, and tetrahedral $[BO_4]^{5-}$.[25–32] These FBBs, through diverse coordination with oxygen atoms, not only contribute to structural diversity but also facilitate the

Tianjin Key Laboratory of Functional Crystal Materials, Institute of Functional Crystal, Tianjin University of Technology, Tianjin 300384, China.
E-mail: cgli@email.tjut.edu.cn

†Electronic supplementary information (ESI) available: Experimental section, other crystallographic data, direction and magnitude of the dipole moments in $K_{7.5}Lu_{2.5}B_{15}O_{30}$, variable-temperature PXRD curves, and the dihedral angle of $[B_5O_{10}]$ groups. CCDC 2386355. For ESI and crystallographic data in CIF or other electronic format see DOI: https://doi.org/10.1039/d4qi02469a

formation of multifunctional groups or clusters, achieved through corner-sharing, edge-sharing, or face-sharing oxygen atoms. Notable examples include $[B_2O_5]^{4-}$,[33–35] $[B_3O_6]^{3-}$,[36,37] $[B_3O_7]^{5-}$, $[B_4O_{12}]^{12-}$, and $[B_5O_{10}]^{5-}$ groups,[38–40] which can undergo further polymerization to form a rich variety of structural architectures, like one-dimensional (1D) chains, two-dimensional (2D) layers, and three-dimensional (3D) frameworks. Additionally, rare earth elements with fully closed-shell or half-filled 4f orbital electronic configurations, like Sc, Y, La, Gd and Lu, are conducive to wide UV transmission windows due to the absence of d–d and f–f electron transitions.[41] Meanwhile, the presence of favorable distortion in RE–O bond-based motifs facilitates the generation of second-order polarizabilities and SHG responses. In view of this, extensive research has been conducted on rare earth borates, such as $La_2CaB_{10}O_{19}$, $K_xNa_{3-x}La_2B_3O_9$ (x = 2–3), $BaYOBO_3$, and $Rb_2ScB_3O_6F_2$,[42–45] which exhibit an intense SHG response and a wide UV transmission range, positioning them as promising NLO crystals in the UV wavelength region. Recent studies have also revealed a series of NCS rare-earth borates, denoted as $A_7M^{II}RE_2(B_5O_{10})_3$ (A = alkali metal, M^{II} = alkaline-earth metal, RE = rare earth metal),[46] featuring $[B_5O_{10}]^{5-}$ motifs with flexible occupancy at cation sites A, M^{II} and RE. Notably, the majority of these $A_7M^{II}RE_2(B_5O_{10})_3$ compounds have short UV cutoff edges below 200 nm and large bandgaps. Furthermore, the observed NLO effects in these compounds are found to be 0.9 to 1.2 times that of KDP, indicating their potential as NLO materials in the UV and deep-UV regions. Consequently, the exploration of deep-UV NLO crystals has led to the identification of rare earth borates comprising $[B_5O_{10}]^{5-}$ groups as a promising candidate system. It is widely known that chemical substitution is an effective strategy for exploring UV NLO materials, with the potential to yield novel NLO crystals with favorable properties through simultaneous cation substitutions. Building on these principles, a novel rare earth borate NLO crystal, $K_{7.5}Lu_{2.5}B_{15}O_{30}$ (KLBO), has been successfully designed and synthesized by the cosubstitution strategy,[46] in which the alkali metal cation K^+ and rare earth cation Lu^{3+} occupy all the A and RE sites in $A_7M^{II}RE_2(B_5O_{10})_3$. The resulting compound adopts the NCS trigonal space group $R32$ (no. 155) and showcases a distinctive 3D structure comprising $[B_5O_{10}]$ and $[LuO_6]$ groups. This unique characteristic endows KLBO with a large SHG response of 1.2 × KDP and a short UV cutoff edge of 198 nm, corresponding to a large bandgap of 6.3 eV. These findings suggest that KLBO is a potential UV NLO crystal material.

Results and discussion

Compound preparation

A polycrystalline pure phase of the KLBO compound was prepared *via* conventional high-temperature solid-phase synthesis, and the corresponding data are presented in Fig. 1. Notably, the experimental X-ray diffraction (XRD) patterns largely align with the corresponding theoretical patterns, indicating a high phase purity. Two tiny peaks labeled with asterisks observed at approximately 20 and 27 degrees can be attributed to $LuBO_3$ (PDF 13-0481), which belongs to the centrosymmetric space group $C2/c$ and exhibits no NLO response. Additionally, in order to ascertain the thermal stability of KLBO, variable temperature XRD analysis was conducted on the polycrystalline powder samples before and after the melting process. The results presented in Fig. s1† reveal that the diffraction pattern of the sample prior to melting (950 °C) is largely consistent with that calculated from the crystallographic data of KLBO. Upon reaching a temperature of 1000 °C, the resulting sample decomposes into $LuBO_3$, indicating the relatively favorable thermal stability of KLBO.

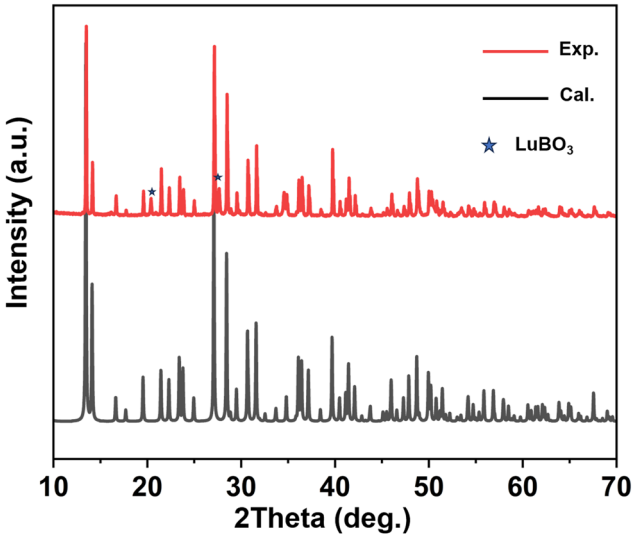

Fig. 1 Experimental and calculated PXRD patterns of KLBO.

Crystal structure

The compound KLBO crystallizes in the acentric $R32$ (no. 155) space group. The cell parameters of KLBO are $a = b$ = 13.1559(6) Å, c = 15.0194(11) Å, V = 2251.3(3) Å^3, $\alpha = \beta$ = 90°, γ = 120° and Z = 1. The asymmetric unit contains four crystallographically independent K atoms, two independent Lu atoms, three independent B atoms, and five independent O atoms. In addition, all atoms except Lu1 with an occupancy of 50.2% and K1 with an occupancy of 49.8% are fully occupied. Tables S1–S3† present the extended crystallographic and refined structural data of KLBO, including information on atomic coordinates and equivalent isotropic displacement parameters, bond lengths, and bond angles. As illustrated in Fig. 2a, the B atoms exhibit two distinct coordination geometries, namely $[BO_4]$ tetrahedra and $[BO_3]$ coplanar triangles. The length of the B–O bond varies from 1.306 Å to 1.469 Å, while the O–B–O bond angle varies from 108.2° to 123.9°. One $[BO_4]$ and four $[BO_3]$ units are further connected by corner-sharing oxygen atoms to form $[B_5O_{10}]$ clusters. Moreover, the isolated $[B_5O_{10}]$ groups with varying orientations extend indefinitely along the ac plane, as illustrated in Fig. 2b. The dihedral angle of the

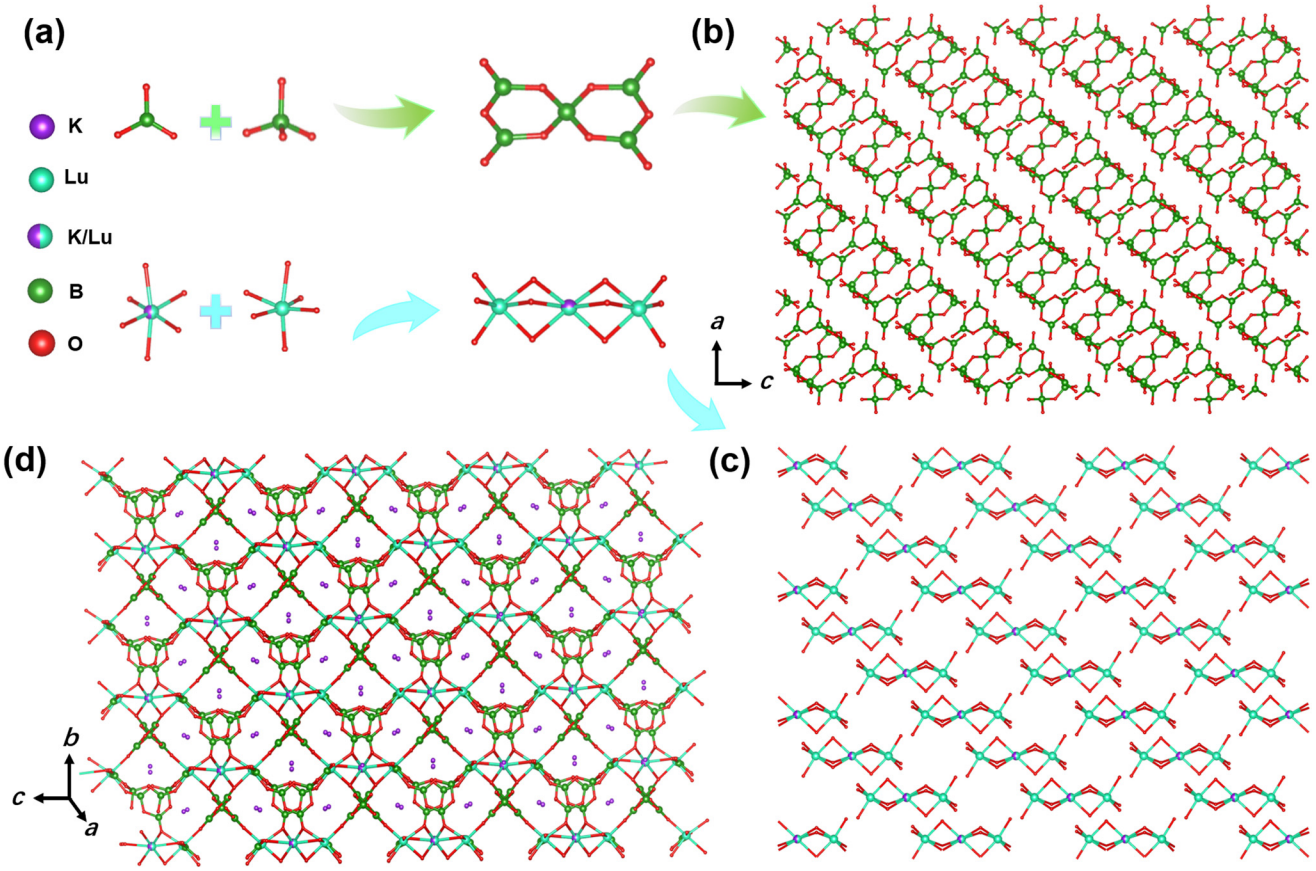

Fig. 2 Structure of KLBO. (a) $[BO_3]$, $[BO_4]$ units, $[B_5O_{10}]$ groups and $[K_{0.5}Lu_{2.5}O_{12}]$ functional building fragments. (b and c) Presentation of the $[B_5O_{10}]$ and $[K_{0.5}Lu_{2.5}O_{12}]$ groups, respectively. (d) 3D structural network.

$[B_5O_{10}]$ motif is shown in Fig. s2.† The Lu atoms coordinate with six O atoms to form $[LuO_6]$ polyhedra, which are interconnected by face-shared oxygen atoms to create a $[K_{0.5}Lu_{2.5}O_{12}]$ cluster (Fig. 2c). This observation is due to the co-occupation of the Wyckoff site by K^+ and Lu^{3+} cations. The length of the Lu–O bond is found to be in the range of 2.174 Å to 2.418 Å and the O–Lu–O bond angle varies from 73.2° to 168.1°. It should be noted that each $[B_5O_{10}]$ group is connected by six $[K_{0.5}Lu_{2.5}O_{12}]$ triangular prisms, which extend indefinitely in different directions to form a 3D structural network, as illustrated in Fig. 2d. The K atoms are aligned along the *c*-direction of the framework channel for charge balancing. Furthermore, bond valence sum (BVS) analysis on KLBO showed that the calculated average valence states of K, Lu, B, and O were found to be 1.23, 2.87, 3.1 and 2.0, respectively, all falling within the anticipated range.

Optical characterization

The transparency range of the KLBO compound was determined through UV-Vis-NIR diffuse reflectance measurements. The alkali metals and rare earth elements possess closed-shell electronic configurations that do not involve d–d or f–f electron transition,[41] which contributes to the blue shift of the UV cutoff edges. As illustrated in Fig. 3a, KLBO maintains high transparency in the wavelength range of 200–2000 nm, with a UV cutoff edge at 198 nm. Consequently, this result corresponds to a wide experimental bandgap of approximately 6.3 eV. Notably, the cutoff edge observed in KLBO is comparable to that of other rare earth borate NLO crystals containing $[B_5O_{10}]$ groups, such as $K_7CaY_2(B_5O_{10})_3$ (below 190 nm),[46] $K_3YB_6O_{12}$ (195 nm), and $K_6Li_3Sc_2B_{15}O_{30}$ (190 nm).[47] This observation indicates the potential of KLBO as a material for NLO applications, particularly in the UV or even deep-UV region. Furthermore, the IR spectra of the KLBO polycrystalline samples were experimentally recorded, as illustrated in Fig. 3b. Notably, distinctive absorption bands are observed at approximately 1384, 1258, and 1200 cm^{-1}, which are ascribed to the asymmetric stretching of the $[BO_3]$ groups. The peak at 930 cm^{-1} is attributed to the symmetric stretching vibration of the $[BO_3]$ unit. The band observed at 1032 cm^{-1} is primarily ascribed to the asymmetric stretching vibration of the $[BO_4]$ unit. The symmetric stretching vibration peaks of the $[BO_4]$ unit are located at 786 and 732 cm^{-1}, while a distinct peak at 616 cm^{-1} is associated with the bending vibration of the $[BO_3]$ and $[BO_4]$ units.[46] These findings are corroborated by previously reported results, providing further support for the rationality of the structural analysis conducted on KLBO.

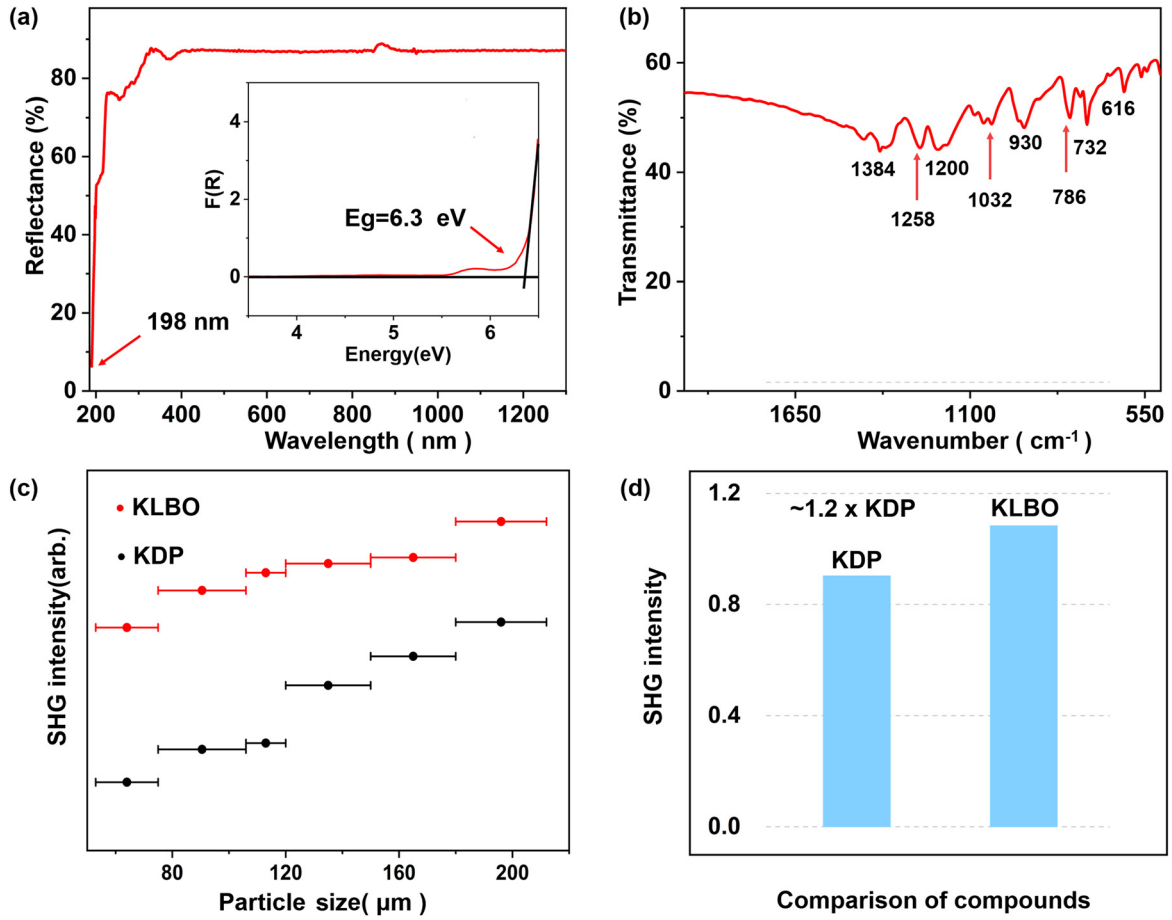

Fig. 3 (a) UV–vis–NIR diffuse reflectance spectrum and the corresponding band gap for KLBO. (b) IR spectrum of KLBO. (c) Phase-matching SHG signals for KLBO and standard KDP with 1064 nm laser radiation. (d) Comparison of SHG between KLBO and KDP.

NLO measurements

The NCS crystal structure of KLBO indicates its potential to exhibit second-order NLO properties. In accordance with the anionic group theory of NLO activity in borates, the planar triangular [BO_3] groups in KLBO are expected to generate a considerable SHG effect, whereas the [BO_4] groups have smaller contributions. The orientation of these groups also plays a role in determining the overall NLO activity. As illustrated in Fig. 3c, the SHG strength of KLBO demonstrates a notable increase with increasing particle size, ultimately reaching a saturation value. This observation suggests that KLBO exhibits a phase matching behavior. Moreover, Fig. 3d demonstrates that KLBO exhibits a large SHG efficiency of ~1.2 × KDP within the particle size range of 180–212 μm, which is comparable to that of other rare earth borate NLO crystals containing [B_5O_{10}] groups, such as $K_7BaSc_2B_{15}O_{30}$ (1.4 × KDP), $K_7SrY_2B_{15}O_{30}$ (1.1 × KDP), and $Rb_3YB_6O_{12}$ (0.8 × KDP).[48] These findings indicate that KLBO exhibits sufficient SHG response to be considered a potential NLO crystal in the UV wavelength range.

Structure–property correlations

To unravel the origin of optical properties observed in KLBO, we performed first-principles calculations based on DFT to study its electronic structures. As shown in Fig. 4a, analysis of the band structure reveals that the valence band (VB) maximum and the conduction band (CB) minimum of KLBO are located at different *k*-points within the Brillouin zone, indicating that it is an indirect band gap compound. The calculated bandgap of KLBO is determined to be 4.6 eV. Furthermore, the maps of the density of states (DOS) and partial density of states (PDOS) in Fig. 4b provide a visual representation of the distribution of electronic orbitals in KLBO. The hybridization of the electronic orbitals in the VB region from the Fermi energy level down to −8 eV primarily involves the s and p orbitals of B and the p orbitals of O, suggesting that the orbitals in the VB region are mainly from the B–O bond-based units. On the other hand, the electronic orbitals in the CB region from 5 to 10 eV are primarily determined by the d orbitals of Lu and the p orbitals of B. It is worth noting that the optical properties of KLBO are mainly determined by the electronic transition between the VB maximum and the CB minimum. Based on the above analyses, it is concluded that the SHG effect originates from the synergistic effect of the B–O and Lu–O bond-based groups. In addition, the dipole moments surrounding the [BO_3] planar triangles and [BO_4] tetrahedra as well as the [LuO_6] octahedra of KLBO were further analyzed. Our analysis revealed that the primary contri-

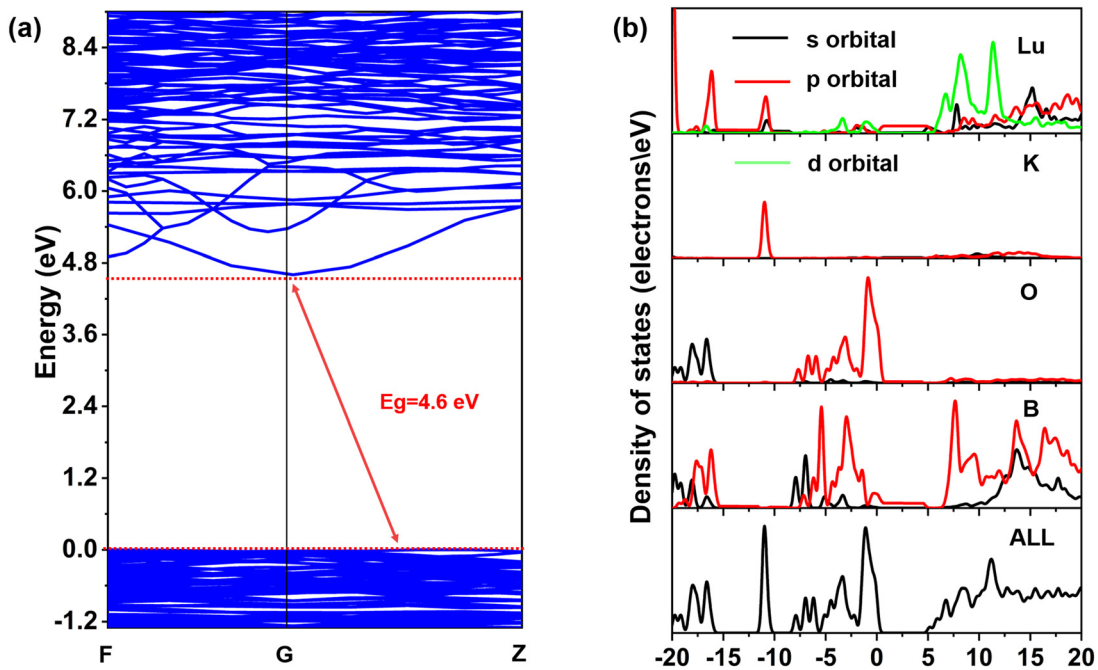

Fig. 4 (a) Band structure for the KLBO crystal. (b) PDOS and TDOS for the KLBO crystal.

butors to the SHG intensity in KLBO are the π-conjugated [BO_3] planar triangles and the distortive [LuO_6] octahedra. Conversely, the non-π-conjugated [BO_4] tetrahedra make a relatively smaller contribution to the overall SHG activities, primarily due to their smaller dipole moments (Table S4†). Consequently, the NLO-active [BO_3] motifs and [LuO_6] octahedra serve as the main contributors to the NLO properties of the KLBO compound.

Conclusions

In conclusion, an alkali metal rare-earth borate NLO crystal, KLBO, was successfully synthesized *via* spontaneous crystallization. A structural analysis of the compound reveals its adoption of the trigonal space group *R*32 (no. 155), featuring a distinctive 3D framework comprising [LuO_6] octahedra and [B_5O_{10}] groups. Notably, UV-Vis-NIR diffuse reflectance analysis demonstrated that KLBO exhibits a significantly short UV absorption cutoff edge below 200 nm, with a wide energy gap of 6.3 eV. Furthermore, KLBO displays an amplified SHG efficiency of 1.2 times that of KDP. Additional insights from structural and theoretical results indicate that the SHG activity of KLBO is primarily derived from the presence of [BO_3] units and distorted [LuO_6] octahedra. These favorable characteristics position KLBO as a promising candidate for NLO applications in the UV wavelength region.

Data availability

The data supporting this article have been included as part of the ESI.†

Crystallographic data for 2386355 have been deposited at the CCDC.†

Conflicts of interest

There are no conflicts to declare.

Acknowledgements

This work was financially supported by the National Key R&D Program of China (2021YFA0717800) and the National Natural Science Foundation of China (Grant No. 62475191, 52002273, and 62104124).

References

1 P. Halasyamani and K. Poeppelmeier, Noncentrosymmetric Oxides, *Chem. Mater.*, 1998, **10**, 2753–2769.
2 F. Liang, L. Kang, P. Gong, Z. Lin and Y. Wu, Rational Design of Deep-Ultraviolet Nonlinear Optical Materials in Fluorooxoborates: Toward Optimal Planar Configuration, *Chem. Mater.*, 2017, **29**, 7098–7102.
3 M. Mutailipu, K. Poeppelmeier and S. Pan, Borates: a rich source for optical materials, *Chem. Rev.*, 2021, **121**, 1130–1202.
4 (*a*) G. Zou and K. Ok, Novel ultraviolet (UV) nonlinear optical (NLO) materials discovered by chemical substitution-oriented design, *Chem. Sci.*, 2020, **11**, 5404–5409;

(*b*) X. Meng, H. Tian, Q. Wu and M. Xia, Nonlinear optical cyanurate crystals, *J. Cryst. Growth*, 2024, **648**, 127930.

5 (*a*) M. Mutailipu, J. Han, Z. Li, F. Li, J. Li, F. Zhang, X. Long, Z. Yang and S. Pan, Achieving the Full-wavelength Phase-matching for Efficient Nonlinear Optical Frequency Conversion in $C(NH_2)_3BF_4$, *Nat. Photonics*, 2023, **17**, 694–701; (*b*) Y. Fu, F. Liang, C. He, H. Yu, H. Zhang and Y. Chen, Photon-phonon collaboratively pumped laser, *Nat. Commun.*, 2023, **14**, 8110.

6 (*a*) P. Yu, L. Wu, L. Zhou and L. Chen, Deep-Ultraviolet Nonlinear Optical Crystals: $Ba_3P_3O_{10}X$ (X = Cl, Br), *J. Am. Chem. Soc.*, 2014, **136**, 480–487; (*b*) F. Liang, C. He, D. Lu, Q. Fang, Y. Fu, H. Yu, H. Zhang and Y. Chen, Multiphonon-assisted lasing beyond the fluorescence spectrum, *Nat. Phys.*, 2022, **18**, 1312–1316; (*c*) Y. Cheng, F. Liang, D. Lu, J. Feng, G. Zhang, H. Yu, H. Zhang and Y. Wu, Phonon engineering in Yb: $La_2CaB_{10}O_{19}$ crystal for extended lasing beyond the fluorescence spectrum, *Light:Sci. Appl.*, 2023, **12**, 203.

7 C. Chen, G. Wang, X. Wang and Z. Xu, Deep-UV nonlinear optical crystal $KBe_2BO_3F_2$-Discovery, growth, optical properties and applications, *Appl. Phys. B: Lasers Opt.*, 2009, **97**, 9–25.

8 B. Wu, D. Tang, N. Ye and C. Chen, Linear and nonlinear optical properties of the $KBe_2BO_3F_2$ (KBBF) crystal, *Opt. Mater.*, 1996, **5**, 105–109.

9 T. Tran, H. Yu, J. Rondinelli, K. Poeppelmeier and P. Halasyamani, Deep ultraviolet nonlinear optical materials, *Chem. Mater.*, 2016, **28**, 5238–5258.

10 M. Mutailipu, M. Zhang, Z. Yang and S. Pan, Targeting the Next Generation of Deep-Ultraviolet Nonlinear Optical Materials: Expanding from Borates to Borate Fluorides to Fluorooxoborates, *Acc. Chem. Res.*, 2019, **52**, 791–801.

11 W. Xie, R. Tang, S. Yan, N. Ma, C. Hu and J. Mao, $Ba_4B_{14}O_{25}$: A Deep Ultraviolet Transparent Nonlinear Optical Crystal with Strong Second Harmonic Generation Response Achieved by a Boron-Rich Closed-Loop Strategy, *Small*, 2024, **20**, e2307072.

12 G. Shi, Y. Wang, G. Zhang, B. Zhang, Z. Yang, X. Hou, S. Pan and K. Poeppelmeier, Finding the Next Deep-Ultraviolet Nonlinear Optical Material: $NH_4B_4O_6F$, *J. Am. Chem. Soc.*, 2017, **39**, 10645–10648.

13 Y. Huang, L. Wu, X. Wu, L. Li, L. Chen and Y. Zhang, $Pb_2B_5O_9I$: An Iodide Borate with Strong Second Harmonic Generation, *J. Am. Chem. Soc.*, 2010, **132**, 12788–12789.

14 (*a*) H. Huang, J. Yao, Z. Lin, X. Wang, R. He, W. Yao, N. Zhai and C. Chen, $NaSr_3Be_3B_3O_9F_4$: A Promising Deep-Ultraviolet Nonlinear Optical Material Resulting from the Cooperative Alignment of the $[Be_3B_3O_{12}F]_{10}$ Anionic Group, *Angew. Chem., Int. Ed.*, 2011, **50**, 9141–9144; (*b*) H. Huang, L. Liu, S. Jin, W. Yao, Y. Zhang and C. Chen, Deep-Ultraviolet Nonlinear Optical Materials: $Na_2Be_4B_4O_{11}$ and $LiNa_5Be_{12}B_{12}O_{33}$, *J. Am. Chem. Soc.*, 2013, **135**, 18319–18322.

15 X. Dong, Q. Jing, Y. Shi, Z. Yang, S. Pan, K. Poeppelmeier, J. Young and J. Rondinelli, $Pb_2Ba_3(BO_3)_3Cl$: A Material with Large SHG Enhancement Activated by Pb-Chelated BO_3 Groups, *J. Am. Chem. Soc.*, 2015, **137**, 9417–9422.

16 M. Xia, X. Jiang, Z. Lin and R. Li, "All-Three-in-One": A New Bismuth–Tellurium–Borate Bi_3TeBO_9 Exhibiting Strong Second Harmonic Generation Response, *J. Am. Chem. Soc.*, 2016, **138**, 14190–14193.

17 C. Chen, Y. Wang, Y. Xia, B. Wu, D. Tang, K. Wu, W. Zeng, L. Yu and L. Mei, New development of nonlinear optical crystals for the ultraviolet region with molecular engineering, *J. Appl. Phys.*, 1995, **77**, 2268–2272.

18 L. Kang, S. Luo, G. Peng, N. Ye, Y. Wu, C. Chen and Z. Lin, First Principles Design of a Deep-Ultraviolet Nonlinear Optical Crystal from $KBe_2BO_3F_2$ to $NH_4Be_2BO_3F_2$, *Inorg. Chem.*, 2015, **54**, 10533–10535.

19 H. Lee and K. Ok, $Na_2Mg_{1-x}Zn_xSiO_4$ ($0 \leq x \leq 1$): Noncentrosymmetric Sodium Metal Silicate Solid Solutions with Ultraviolet Nonlinear Optical Properties, *Bull. Korean Chem. Soc.*, 2020, **41**, 139–142.

20 Y. Li, W. Huang, Y. Zhou, X. Song, J. Zheng, Y. Wang, Y. Song, M. Li, J. Luo and S. Zhao, A High-Performance Nonlinear Optical Crystal with a Building Block Containing Expanded π-Delocalization, *Angew. Chem., Int. Ed.*, 2023, **62**, e202215145.

21 C. Chen, Y. Wu, A. Jiang, B. Wu, G. You, R. Li and S. Lin, New nonlinear-optical crystal: LiB_3O_5, *J. Opt. Soc. Am. B*, 1989, **6**, 616–621.

22 C. Chen, B. Wu, A. Jiang and G. You, A new-type ultraviolet SHG crystal—*β*-BaB_2O_4, *Sci. Sin., Ser. B*, 1985, **28**, 235.

23 Y. Wu, T. Sasaki, S. Nakai, A. Yokotani, H. Tang and C. Chen, CsB_3O_5: A new nonlinear optical crystal, *Appl. Phys. Lett.*, 1993, **62**, 2614–2615.

24 (*a*) J. Tu and D. Keszler, $CsLiB_6O_{10}$: A noncentrosymmetric polyborate, *Mater. Res. Bull.*, 1995, **30**, 209–215; (*b*) Y. Mori, I. Kuroda, S. Nakajima, T. Sasaki and S. Nakai, New nonlinear optical crystal: Cesium lithium borate, *Appl. Phys. Lett.*, 1995, **67**, 1818–1820.

25 X. Pan, H. Wu, S. Cheng and Z. Wang, $Pb_3Ba_3Zn_6(BO_3)_8$ and *α*-$BaZn_2(BO_3)_2$: new members of the zincoborates containing two different dimensional Zn–O units, *Inorg. Chem. Front.*, 2020, **7**, 101–107.

26 Y. Wang, B. Zhang, Z. Yang and S. Pan, Cation-Tuned Synthesis of Fluorooxoborates: Towards Optimal Deep-Ultraviolet Nonlinear Optical Materials, *Angew. Chem.*, 2018, **130**, 2172–2176.

27 M. Xia and R. Li, Growth, structure and optical properties of nonlinear optical crystal $BaZnBO_3F$, *J. Solid State Chem.*, 2016, **233**, 58–61.

28 X. Wang, F. Zhang, L. Gao, Z. Yang and S. Pan, Nontoxic KBBF Family Member $Zn_2BO_3(OH)$: Balance between Beneficial Layered Structure and Layer Tendency, *Adv. Sci.*, 2019, **6**, 1901679.

29 M. Fabian and E. Svab, Formation of Mixed Bond-Angle Linkages in Zinc Boromolybdate Glasses, *J. Am. Ceram. Soc.*, 2016, **99**, 2292–2299.

30 X. Xu, C. Hu, F. Kong, J. Zhang and J. Mao, $Ca_{10}Ge_{16}B_6O_{51}$ and $Cd_{12}Ge_{17}B_8O_{58}$: Two Types of New 3D Frameworks

Based on BO_4 Tetrahedra and 1D $[Ge_4O_{12}]_n$ Chains, *Inorg. Chem.*, 2011, **50**, 8861–8868.

31 W. Li, H. Wu, H. Yu, Z. Hu, J. Wang and Y. Wu, $Ba_6BO_3Cl_9$ and $Pb_6BO_4Cl_7$: structural insights into ortho-borates with uncondensed BO_4 tetrahedra, *Chem. Commun.*, 2020, **56**, 6086–6089.

32 Y. Zhang, F. Li, R. Yang, Y. Yang, F. Zhang, Z. Yang and S. Pan, $Rb_5Ba_2(B_{10}O_{17})_2(BO_2)$: The formation of unusual functional $[BO_2]^-$ in borates with deep ultraviolet transmission window, *Sci. China:Chem.*, 2022, **65**, 719–725.

33 J. Ju, T. Yang, G. Li, F. Liao, Y. Wang, L. You and J. Lin, PKU-5: An Aluminoborate with Novel Octahedral Framework Topology, *Chem. – Eur. J.*, 2004, **10**, 3901–3906.

34 S. Li, X. Liu, H. Wu, Z. Song, H. Yu, Z. Lin, Z. Hu, J. Wang and Y. Wu, $Ba_4Ca(B_2O_5)_2F_2$: π-conjugation of B_2O_5 in the planar pentagonal layer achieving large second harmonic generation of pyro-borate, *Chem. Sci.*, 2021, **12**, 13897–13901.

35 J. Zhang, C. Hu, X. Xu, F. Kong and J. Mao, New Second-Order NLO Materials Based on Polymeric Borate Clusters and GeO_4 Tetrahedra: A Combined Experimental and Theoretical Study, *Inorg. Chem.*, 2011, **50**, 1973–1982.

36 Z. Jia, N. Zhang, Y. Ma, L. Zhao, M. Xia and R. Li, Top-Seeded Solution Growth and Optical Properties of Deep-UV Birefringent Crystal $Ba_2Ca(B_3O_6)_2$, *Cryst. Growth Des.*, 2017, **17**, 558–562.

37 Z. Fang, X. Jiang, M. Duan, Z. Hou, C. Tang, M. Xia, L. Liu, Z. Lin, F. Fan, L. Bai and C. Chen, Deep-Ultraviolet Nonlinear Optical Crystal $Cs_2Al_2(B_3O_6)_2O$: A Benign Member of the $Sr_2Be_2(BO_3)_2O$ Family with $[Al_2(B_3O_6)_2O]^{2-}$ Double Layers, *Chem. – Eur. J.*, 2018, **24**, 7856–7860.

38 C. Chen, Y. Wang, B. Wu, K. Wu, W. Zeng and L. Yu, Design and synthesis of an ultraviolet-transparent nonlinear optical crystal $Sr_2Be_2B_2O_7$, *Nature*, 1995, **373**, 322–324.

39 R. Tang, C. Hu, F. Mao, J. Feng and J. Mao, $Ba_4Bi_2(Si_{8-x}B_{4+x}O_{29})$ (x = 0.09): a new acentric metal borosilicate as a promising nonlinear optical material, *Chem. Sci.*, 2019, **10**, 837–842.

40 (*a*) K. Feng, W. Yin, W. Hao, J. Yao and Y. Wu, A novel UV nonlinear optical crystal material: $K_{21}Yb_8B_{45}O_{90}$, *CrystEngComm*, 2013, **15**, 5064–5069; (*b*) J. Zhou and R. Li, A non–centrosymmetric compound $K_7Li_2Y_2B_{15}O_{30}$ by introducing more alkali metals into $A_7MRe_2B_{15}O_{30}$ family, *J. Solid State Chem.*, 2021, **304**, 122630.

41 R. Liu, H. Wu, H. Yu, Z. Hu, J. Wang and Y. Wu, $K_5Mg_2La_3(BO_3)_6$: An Efficient, Deep-Ultraviolet Nonlinear Optical Material, *Chem. Mater.*, 2021, **33**, 4240–4246.

42 J. Feng, F. Fan, Y. Chen, W. Liu, J. Shen, G. Zhang and H. Tu, Growth and characterizations of $La_2CaB_{10}O_{19}$ crystal from the new $Li_2B_4O_7$–MoO_3 flux system with lower volatility and viscosity, *J. Cryst. Growth*, 2021, **576**, 126383.

43 J. Song, H. Zhao, C. Li, N. Ye, Z. Hu and Y. Wu, A-site cation manipulation of exemplary second harmonic generation response and optical anisotropy in rare-earth borates, *Chem. Sci.*, 2024, **15**, 16196–16204.

44 M. Gao, H. Wu, H. Yu, Z. Hu, J. Wang and Y. Wu, $BaYOBO_3$: A deep-ultraviolet rare-earth oxy-borate with a large second harmonic generation response, *Sci. China: Chem.*, 2021, **64**, 1184–1191.

45 Q. Zhang, R. An, X. Long, Z. Yang, S. Pan and Y. Yang, Exploiting Deep-Ultraviolet Nonlinear Optical Material $Rb_2ScB_3O_6F_2$ Originated from Congruously Oriented $[B_3O_6]$ Groups, *Angew. Chem., Int. Ed.*, 2024, e202415066.

46 (*a*) M. Mutailipu, Z. Xie, X. Su, M. Zhang, Y. Wang, Z. Yang, M. Janjua and S. Pan, Chemical Cosubstitution-Oriented Design of Rare-Earth Borates as Potential Ultraviolet Nonlinear Optical Materials, *J. Am. Chem. Soc.*, 2017, **139**, 18397–18405; (*b*) Z. Xie, M. Mutailipu, G. He, G. Han, Y. Wang, Z. Yang, M. Zhang and S. Pan, A Series of Rare-Earth Borates $K_7MRE_2B_{15}O_{30}$ (M = Zn, Cd, Pb; RE = Sc, Y, Gd, L.u with Large Second Harmonic Generation Responses, *Chem. Mater.*, 2018, **30**, 2414–2423.

47 (*a*) S. Zhao, G. Zhang, J. Yao and Y. Wu, $K_3YB_6O_{12}$: A new nonlinear optical crystal with a short UV cutoff edge, *Mater. Res. Bull.*, 2012, **47**, 3810–3813; (*b*) S. Zhao, G. Zhang, J. Yao and Y. Wu, $K_6Li_3Sc_2B_{15}O_{30}$: A new nonlinear optical crystal with a short absorption edge, *CrystEngComm*, 2012, **14**, 5209–5214.

48 (*a*) S. Li, W. Li, X. Li, G. Yang, N. Ye, Z. Hu, Y. Wu and C. Li, A bifunctional primitive strategy induces enhancements of large second harmonic generation and wide UV transmittance in rare-earth borates containing $[B_5O_{10}]$ groups, *Chem. Sci.*, 2024, **15**, 8959–8965; (*b*) Z. Jia, Q. Zeng, P. Gong, Y. Dong, X. Zhang, B. Xin, Z. Lin and M. Xia, Nonlinear-Optical Crystal $Rb_3YB_6O_{12}$ with Condensed B_5O_{10} Blocks That Exhibits an Intriguing Structural Arrangement and a Short Ultraviolet Absorption Edge, *Inorg. Chem.*, 2020, **59**, 13029–13033.

